Local-overall interactive buckling of welded stainless steel box section compression members

H.X. Yuan[a],*, Y.Q. Wang[a], L. Gardner[b], Y.J. Shi[a]

[a]*Key Laboratory of Civil Engineering Safety and Durability of China Education Ministry, Department of Civil Engineering, Tsinghua University, Beijing 100084, PR China*

[b]*Department of Civil and Environmental Engineering, Imperial College London, London SW7 2AZ, United Kingdom*

Corresponding author: Dr Huanxin Yuan, School of Civil Engineering, Wuhan University, Wuhan 430072, China. Email: yuanhx@whu.edu.cn

Abstract

The interaction between local and overall buckling of welded stainless steel columns has been investigated experimentally and numerically in this study. Eight stainless steel box section compression members were fabricated from slender hot-rolled plates. The material properties and welding residual stress patterns in the test specimens had been obtained previously. Initial geometric imperfections, both local and global, were accurately measured prior to the tests. The test specimens were axially loaded between two pin-ended supports, and both local plate buckling and overall flexural buckling featured visibly in the observed failure modes. Finite element (FE) models were also set up using the ABAQUS software package to conduct numerical simulations, which were initially validated by means of comparison with the experimental data. Using the validated FE models, parametric studies were carried out to assess the influence of the key input parameters, such as the residual stresses, the material strain hardening exponent and non-dimensional proof stress, geometric imperfections and slenderness ratios. Existing design methods, including the design provisions of Eurocode 3 Part 1.4, the design proposal of Rasmussen and Rondal, the direct strength method (DSM) for cold-formed carbon steel and two revisions thereof, were all evaluated against the obtained test and numerical results. It was revealed that the EN 1993-1-4 buckling curves, which do not differ with grade, provide reasonable average strength predictions, but tend to slightly overpredict the local-overall buckling resistances of welded austenitic stainless steel members and slightly underestimate those of duplex stainless steel members. Furthermore, the three considered DSM design curves, all of which were developed on the basis of structural performance data from cold-formed sections, provide generally unconservative strength predictions for welded stainless steel sections. Based on the generated data points, modifications to the current EN 1993-1-4 provisions and the DSM have been proposed, which offer more accurate strength predictions for local-overall interactive buckling resistances of welded stainless steel box section columns.

Keywords: Box sections; Design; Experiments; Interaction; Local buckling; Numerical modelling; Overall buckling; Stainless steel; Structures; Welded columns

1. Introduction

Stainless steels are being increasingly used in structural applications, particularly those in which the key durability benefits of the material can be exploited [1]. The majority of the previous research on structural stainless steel has focused on the behaviour of cold-formed sections. However, heavier load bearing applications require larger, typically welded sections, for which there is a growing trend. Hence, a study of the behaviour of welded stainless steel box columns, with an emphasis on local-overall interaction buckling [2-4] is the focus of the present paper.

Compression tests on structural stainless steel elements, aimed at studying either overall buckling [5-8] or local

buckling [9-11], have been conducted by many researchers. Interactive buckling of stainless steel members, involving local and global modes, has been studied less extensively, though the following recent investigations have been carried out on cold-formed sections. Young and Lui [12] tested twenty-four cold-formed duplex stainless steel SHS and RHS columns, five of which were reported to fail by interactive buckling. Becque and Rasmussen [13-15] carried out experimental and numerical research on cold-formed stainless steel lipped channel columns and I-section columns and developed design provisions to account for the local-overall interaction buckling effects, while Rossi et al. [16,17] studied combined distortional and overall flexural-torsional buckling of cold-formed stainless steel sections. In addition, Gonçalves and Camotim [18] used the generalised beam theory to analyse the local and global buckling of stainless steel columns. Experiments on welded stainless steel columns, featuring interactive buckling, are scarce. Hence, the present paper involves testing of such members, and assesses the applicability of existing methods to their design.

Interactive buckling tests on a total of eight welded stainless steel columns with box sections were conducted in this study, exploring the local-overall buckling behaviour and resistances. The material properties, initial geometric imperfections, both local and global, and welding residual stresses were all measured prior to the tests. The test specimens were axially loaded with pin-ended boundary conditions. The test results were used to validate FE models, which were subsequently used to carry out systematic parametric studies. The obtained test and numerical results are then used to evaluate the current design provisions of EN 1993-1-4 [19], the DSM for carbon steel [20, 21] and two revised versions thereof proposed by Becque et al. [15] and Huang and Young [22] for stainless steel. This study also forms part of the fundamental work to underpin the development of the first Chinese design code for structural stainless steel.

2. Material properties and test specimens

Two stainless steel alloys – austenitic grade EN 1.4301 and duplex grade EN 1.4462, were examined in this study. The material properties were obtained from tensile and compressive coupon tests, which were reported in a previous study [23]. Table 1 lists the material properties of the 6.00 mm plates, from which all of the test specimens were fabricated, while the full recorded stress-strain curves are plotted in Fig. 1. It can be seen that the austenitic EN 1.4301 alloy exhibits more considerable strain-hardening behaviour while the duplex EN 1.4462 alloy is of higher strength.

The measured average geometric dimensions of the test specimens are tabulated in Table 2, in which λ_{pf} and λ_{pw} are local element slendernesses for the flanges and the webs, respectively and λ_c is the non-dimensional global member slenderness; each of these is defined as the square root of the ratio of the yield to elastic buckling stress of the element or member. Other symbols are defined in Fig. 2. The cross-sections of the test specimens were designed to be of slender proportions, and hence susceptible to local plate buckling. The nominal outer sectional dimensions ranged from 180 mm to 400 mm, covering a wide range of plate width-to-thickness ratios from 28.0 to 64.7. Three cross-sectional aspect ratios h/b_f of 1.0, 1.5 and 2.0 were included. The effective length (L_e) of the columns was taken as the geometric length (L) plus the depth of the two pinned ends (2×190 mm=380 mm). The slenderness ratio (L_e/r_y) of the test specimens varied from 40.7 to 57.0, which corresponds to columns of intermediate slenderness. All the web plates were machined to create beveled edges for butt welds. The test specimens were fabricated from hot-rolled plates by means of shielded metal arc welding (SMAW) and the weld size was designed to be 5 mm. All the constitutive plates of the test specimens studied in this paper were cut parallel to the longitudinal coil direction. Both ends of each test specimen were fitted with two 20 mm thick carbon steel end plates.

3. Determination of initial imperfections and residual stresses

Prior to testing, the initial global and local imperfections, together with the residual stresses, in the test specimens

were measured, as described in the following sub-sections.

3.1 Global geometric imperfections

By means of an optical theodolite and a calibrated vernier caliper, the initial global geometric imperfections were measured [24]. A schematic view and field photo of the measurement setup are shown in Fig. 3. On the basis of a virtual straight line generated from the theodolite, five cross-sections – the mid-length section, two quarter point sections and two end sections, were measured along each column specimen for determining the amplitude of the initial global curvature. Due to the restriction of the end plates, the two end sections were moved 50 mm away from the end plates. The maximum deviation from a straight line between the two ends of the members was taken as the global imperfection amplitude, $v_0=\max(v_1, v_2, v_3)$. Based on the described method, the global geometric imperfections were measured and are summarised in Table 3. It can be observed that the overall geometric imperfections of the test specimens are generally small, with the maximum amplitude reaching only $L/2000$.

3.2 Local geometric imperfections

The local imperfections of the test specimens were measured using the tool [20] shown in Fig. 4, which involved a digital linearly-varying displacement transducer (LVDT), driven by a calibrated electric guideway at a constant rate (2 mm/s), recording positional data across the section and corresponding time points. Three cross-sections – the mid-length cross-section and two quarter point cross-sections were measured for each constitutive plate. The local imperfection amplitude (w_0) for each specimen was taken as the maximum value among the three cross-sections. The measured results are summarised in Table 3.

3.3 Residual stress patterns

Residual stress measurements were taken on additional samples fabricated in parallel with the test specimens and using the same welding process. Measurements were taken by means of the sectioning method. Based on the ECCS predictive model [25] for welded carbon steel sections, a new predictive model for determining the residual stresses in welded stainless steel box sections was proposed [26]. The basic distribution pattern is shown in Fig. 5, while Table 4 lists the key parameters of the newly proposed model, which shows lower peak tensile residual stresses, narrower peak tension zones but wider transition zones, compared with the existing models for carbon steel structural sections.

4. Interactive buckling tests

4.1 Test set-up

The test set-up and instrumentation scheme for the interactive buckling tests was devised by referring to [27]. For each test specimen, the five cross-sections employed in the measurement of global geometric imperfections were used again as measuring points, and there were a total of 13 LVDTs and 32 strain gauges for each specimen, as illustrated in Fig. 6. Specifically, LVDTs 1 and 2 measured the end-shortening of the test specimens between the two pinned ends; LVDTs 3 and 4 and LVDTs 5 and 6 were used to determine the upper and lower end rotations, respectively; all other LVDTs recorded the lateral deflections. The attached strain gauges were used to align the test specimens and to monitor the onset and progression of local plate buckling. The test specimens were axially loaded using a 5000 kN capacity hydraulic testing machine between two pin-ended supports, which were free to rotate about the y-axis only. The welded end plates provided good contact between the test column and the pinned ends, avoiding possible localised failure of the column ends.

Two steps were taken to align the test columns. Firstly, geometrical centreing was implemented by means of a laser, coupled with the achievement of close contact between the end plates and supports. In the second step, a

preloading procedure was undertaken up to around 10% of the estimated ultimate load. The strain readings from the mid-length and quarter point cross-sections were used to assess the alignment and make further adjustments. Once the alignment work was completed, a small axial load of approximately 5 kN was maintained to eliminate any possible gaps between the upper end plate and the corresponding support.

The tests were initially load controlled, at a rate of 90 kN per minute; after ultimate load, the test was switched to displacement control, at a rate of 25 mm per minute. The test was continued beyond ultimate load, enabling the post-ultimate response to be recorded. All the readings were recorded at one second intervals by a data acquisition system developed at Tsinghua University. Fig. 7 displays the overall test set-up and interactive failure mode of specimen R304-400-i.

4.2 Load eccentricity

The initial load eccentricity applied to each test specimen about the minor axis (y axis) can be estimated by means of the strain gauges readings at the two quarter point cross-sections. The obtained axial stress state can be separated into two simple states – pure axial compression (σ_F) and pure bending (σ_M), as illustrated in Fig. 8. For each cross-section, the internal axial force F and the moment M are given by Eq. (1).

$$\begin{cases} F = \sigma_F A = EA\varepsilon_F \\ M = \sigma_M W_{el} = EW_{el}\varepsilon_M \end{cases} \tag{1}$$

in which ε_F and ε_M correspond to the strains generated by pure axial compression (σ_F) and pure bending (σ_M), respectively, E is the material Young's modulus, A is the cross-section area and W_{el} is the elastic section modulus. Hence the initial load eccentricity e_c can be computed from

$$e_c = \frac{M}{F} = \frac{W_{el}}{A} \frac{\varepsilon_M}{\varepsilon_F} \tag{2}$$

In view of the possible difference in load eccentricity between the top and bottom ends, the load eccentricity of each test specimen was averaged between the lower and upper end cross-sections, as listed in Table 3. The equivalent initial eccentricity e_{Eq} of a column may be approximated as the sum of the loading eccentricity e_c plus initial geometric imperfections v_0:

$$e_{Eq} = e_c + v_0 \tag{3}$$

which had a maximum value of $L/394$ for specimen R304-360-i, with an average value of $L/1241$ for all the test specimens.

4.3 Test results

All the test specimens experienced local-overall interaction buckling, as presented in Fig. 9. Typically, the test specimens exhibited first local buckling, followed by overall buckling. Under increasing load, and as the overall lateral deflections grew, the local buckles on the tension (or less heavily compressed) side of the member were eased while those on the other side developed further, as illustrated in Fig. 7 (b). The axial load versus end shortening and mid-length lateral deflection curves were recorded for all test specimens, and are shown in Figs. 10 and 11. The ultimate test load-carrying capacities and corresponding deformation values are summarised in Table 5.

The experimentally observed elastic critical local buckling loads were also determined by means of the strain gauge readings using the maximum surface strain method [28]. According to this method, the critical local buckling load corresponds to the reversal point at which the compressive strain on the plate surface begins to reduce with increasing axial load [29]. This reversal point on the axial load-strain curves (plotted in Fig. 12) was acquired at the three intermediate measurement locations – Z2-Z2, Z3-Z3 and Z4-Z4, shown in Fig. 6. The minimum value of critical local buckling loads from these three measurement locations was taken as the critical local buckling load N_{crl} of the column. In view of the fact that the attached strain gauges may or may not coincide with the exact point of

initiation of local plate buckling, the obtained critical local buckling load may be considered as an upper bound value, although it has been found that this method often offers more conservative predictions compared with other measures [30]. By adopting this method, the critical local buckling loads N_{crl} for all the test specimens were obtained and are summarised in Table 6. As expected, the N_{crl} values for the grade EN 1.4301 specimens are close to the corresponding values for the grade EN 1.4462 specimens due to its dependency on elastic stiffness and geometric dimensions, rather than material strength. The obtained experimental buckling stresses were found to be lower than the theoretical values determined on the basis of elastic assumptions; this is attributed primarily to the low material proportionality limit of stainless steel and the non-linear material behaviour [31], but may also be related to other factors including welding residual stresses, initial geometric imperfections, load eccentricities and global bending deformations.

The obtained test results are used in the next section to validate numerical models, after which parametric studies are performed. The combined experimental and numerical data set is used in the assessment and development of design guidance in Section 6.

5. Numerical modelling of interactive buckling

5.1 Numerical models

Numerical models were developed using the FE software package ABAQUS [32], with the initial aim of simulating the results achieved in the test programme. The measured material properties, initial local and global geometric imperfections, residual stress patterns and initial load eccentricities were all incorporated into the FE models.

Measured longitudinal tension (LT) material properties were used in the numerical models in favour of the longitudinal compression (LC) values, which were also measured, due to greater confidence in their accuracy, the availability of data to higher strains, and the relatively similar results between the tension and compression material properties. The modified Ramberg-Osgood material model proposed by Gardner and Ashraf [33] has been shown to provide accurate predictions of both tension and compression stress-strain curves and was fitted to the measured stress-strain data to give a single smooth curve, which was then used in the subsequent numerical modelling. The widely adopted shell element with reduced integration, S4R, was used to mesh the box section columns. This element has been successfully used in numerical modelling of welded stainless steel sections [34] and the buckling response of structural stainless steel components [35, 36].

The longitudinal element size was around 30 mm, while the corresponding element widths conformed to the widths of the strips in the residual stress model. This facilitated consistent element aspect ratios, which played an important role in reaching a converged solution. It was also found out that no more than 0.5% improvement in accuracy was achieved by introducing a much finer mesh.

The pinned ends in the tests that allowed free rotations about the y-axis of the column cross-section were simulated by applying suitable end boundary conditions – all degrees of freedom at the bottom end of the column were fixed except for the rotation about the minor axis, and four degrees of freedom at the top end were also fixed, leaving the same rotation and the longitudinal displacement free. Two reference points were introduced to implement the boundary conditions, which were then coupled with the corresponding end surfaces, such that the motion of the whole end surface and that of the reference point were the same. Furthermore, each reference point was moved away from the end surface by a distance of 190 mm, accounting for the depth of the pinned end [22]. Hence the effective length (L_e) would be reached by adding the two end depths (380 mm) to the geometric length (L) of the column. Furthermore, the measured load eccentricities e_c could also be considered by moving the reference points away from the minor axis.

Initial local and global geometric imperfections were both included in the FE models. The imperfection shapes

were generated from an initial eigenvalue buckling analysis, with the lowest local and global buckling modes used for local and global imperfections, respectively. The previously measured amplitudes of imperfections were input by means of the *IMPERFECTION command. The local and global geometric imperfections were linearly superposed.

For welded structural members, the presence of residual stresses may reduce the initial stiffness and deteriorate the buckling resistance. Hence, residual stresses were included in the FE models through the *INITIAL CONDITIONS (TYPE=STRESS) command and in the pattern presented in Table 4. The peak tensile residual stresses for the grade EN 1.4301 and EN 1.4462 specimens were taken as $0.8\sigma_{0.2}$ and $0.6\sigma_{0.2}$, respectively. Fig. 13 illustrates the residual stress distributions in the FE models for specimens S304-300-i and R2205-400-i.

5.2 Numerical simulation of the test specimens

Numerical simulations were performed to model the interactive buckling tests described in Section 4, using the Riks method and including geometric nonlinearity. The load-deformation curves obtained by FE modelling were compared with the corresponding test curves, as depicted in Fig. 14. The interactive failure modes involving local and overall buckling from two specimens – R304-360-i and S2205-300-i, are presented in Fig. 15, revealing good agreement between the FE predictions and test results.

The acquired FE results, including the ultimate buckling resistances and corresponding end shortening deformations and mid-length lateral deflections, are all summarised in Table 5. The critical buckling stresses obtained from the FE modelling using the same method as for the tests are listed in Table 6. The comparisons of Table 5 show that the mean value of the buckling resistance ratio $N_{u,FE}/N_{u,Exp}$ is 1.00 with the corresponding coefficient of variation (COV) of 0.02, demonstrating excellent strength predictions provided by the numerical simulations. Meanwhile, it may be seen that the FE models generally slightly underestimate the end shortening deformations yet may overestimate the lateral deflections at ultimate load, with mean values of FE/test displacements of 0.90 and 1.16, respectively. However, given the sensitivity of these values to the various input parameters, this agreement is considered to be satisfactory and overall the numerical models are deemed to provide accurate predictions of the behaviour of welded stainless steel box columns undergoing local-overall interaction buckling.

5.3 Parametric studies

The validated FE models are used herein to carry out systematic parametric studies, revealing the influences of the key input parameters, such as the residual stresses, initial geometric imperfections, material properties, and local and member slenderness. The *PARAMETER command was used to input a range of values of the key parameters during the numerical simulations.

The FE models were run with and without residual stresses. For cold-formed stainless steel columns, it has previously been found that the effect of residual stresses on ultimate load-carrying capacity is small [37, 38], which may be mainly attributed to the fact that the dominant residual stresses in cold-formed sections are those that vary through the thickness (i.e. bending residual stresses), which are inherently present in material stress-strain properties obtained by testing coupons extracted from structural sections [39]. However, the contrast between the simulations with and without residual stresses in the present study was more significant. Comparisons are shown for specimens R304-360-i and S2205-300-i in Fig. 14. Detailed comparisons between test and FE results (with and without residual stresses) for buckling resistances and deformations are listed in Table 5. By disregarding residual stresses, test buckling resistances are overpredicted by an average of 5% by the FE models, while the deformations, both end shortenings and lateral deflections, are substantially underpredicted. Hence, residual stresses cannot be neglected when considering welded stainless steel columns undergoing interactive buckling. This conclusion is further emphasised by the direct comparison of numerical results with and without residual stresses shown in Fig. 16. Herein the ultimate buckling resistance obtained by FE modelling (N_{FE}) was normalised by the effective cross-sectional yield load $N_{eff}=A_{eff}\sigma_{0.2}$, in which A_{eff} is the effective cross-section area calculated by provisions from the EN

1993-1-4 (presented in Section 6), and the global slenderness λ_c is also obtained based on the above effective cross-section area A_{eff}. The enhanced sensitivity of welded box sections to residual stresses, as compared to previously examined cold-formed sections, relates to both their nature (i.e. predominantly axial rather than bending residual stresses) and distribution (tensile stresses in the corner regions and compressive stresses in towards the centre of the flat plates promoting earlier local buckling). Residual stresses were therefore included in all models considered hereafter.

Three different amplitudes of the local geometric imperfection – $b/200$ (corresponding to the recommendation from EN 1993-1-5 [40]), $b/300$ and $b/500$, and three other amplitudes of the global geometric imperfection – $L_e/500$, $L_e/1000$ and $L_e/2000$, were chosen to generate five combinations: $b/200$-$L_e/500$ (most severe combination), $b/200$-$L_e/1000$ (standard combination), $b/300$-$L_e/1000$, $b/500$-$L_e/1000$ and $b/500$-$L_e/2000$ (least severe combination). All five imperfection combinations were considered for both grades EN 1.4301 and EN 1.4462 sections over a wide range of overall slenderness. The detrimental effect on the ultimate buckling resistances by using the different imperfection combinations were analysed, with the comparison presented in Fig. 17. The columns within the intermediate overall slenderness regions exhibited the most diverse buckling resistances, suggesting that these columns are more sensitive to the initial geometric imperfections. It can also be seen that the grade EN 1.4301 sections suffer more severe strength reduction than the grade EN 1.4462 sections, which is attributed mainly to the higher residual stress levels. The standard combination of $b/200$- $L_e/1000$ was used to carry out the subsequent numerical simulations afterwards.

The influence of the material properties, including the Ramberg-Osgood strain hardening exponent n and the non-dimensional proof stress $e=\sigma_{0.2}/E_0$ on interactive buckling resistances, was also considered. In EN 1993-1-4, the values of n vary from 5 to 16 for currently prevalent stainless steel grades, and the values of e range from 0.001 to 0.0024. Meanwhile, based on the measured material properties for grades EN 1.4301 and EN 1.4462 [23], the minimum and maximum values of n were 5.8 and 10.8, respectively, which lie within the range in EN 1993-1-4. However, the measured values of the parameter e ranged from 0.0015 to 0.0033 and exceeded the above range. Hence, in this study, four values of the exponent n (5, 7.5, 10, 16) and five values of the parameter e (0.001, 0.0015, 0.002, 0.0025, 0.0035) were considered. In the models, the peak tensile residual stresses were taken as the $0.6\sigma_{0.2}$ for the high strength alloys (e=0.0025, 0.0035) and $0.8\sigma_{0.2}$ for the three low strength alloys. A constant SHS section, $b_f=h=250$ mm and $t=6$ mm, was chosen to carry out this study. The results of the study to assess the influence of the parameters, n and e, are shown in Figs. 18 and 19. From the results, it may be seen that for a given value of the parameter e, the normalised buckling strength increases with increasing values of n, especially for columns of intermediate slenderness. This effect is more pronounced for the smaller value of e=0.001. Furthermore, increasing the non-dimensional proof stress e generally raises the normalised buckling performance, with greater influence for the smaller values of n.

Having determined suitable imperfection levels and confirmed the need to include residual stresses, a series of parametric studies were considered. Numerical simulations on a total of 312 stainless steel box section columns were carried out, incorporating a wide range of key parameters – element slenderness λ_p (0.62-2.18), global slenderness λ_c (0.33-1.45, based on the effective section properties), aspect ratio of cross-section (1.0, 1.5 and 2.0), exponent n (5-16) and parameter e (0.001-0.0035). The previously measured material properties, represented by the modified Ramberg-Osgood model [33], were used in the FE models. The FE results are summarised and used to assess the design strengths provided by the existing design methods in the following section.

6. Local-overall buckling resistances of the columns

6.1 General

Design methods that cover the buckling resistances of stainless steel columns undergoing local-overall interaction

buckling include the current EN 1993-1-4 provisions [19] and the DSM [20]. These methods, which were both established primarily on the basis of the behaviour of cold-formed steel structures, feature different approaches in relation to the treatment of local buckling. Specifically, while EN 1993-1-4 utilises the classical effective width method and treats sections on an element by element basis, the DSM considers the elastic buckling and yield capacity of the full cross-section [41]. The proposals of Rasmussen and Rondal [42] are also assessed.

6.2 Evaluation of EN 1993-1-4

For class 4 cross-sections under compression, the buckling resistance $N_{b,Rd}$ is defined in EN 1993-1-4 as:

$$N_{b,Rd} = \chi A_{eff} f_y / \gamma_{M1} \tag{4}$$

in which χ is the overall buckling reduction factor, f_y is the material yield strength, taken as $\sigma_{0.2}$, γ_{M1} is the partial factor for member buckling (set equal to unity for all comparisons made herein), and A_{eff} is the effective area of the cross-section, with the corresponding effective width reduction factor ρ given by Eq. (5) for welded internal elements,

$$\rho = \frac{0.772}{\lambda_p} - \frac{0.125}{\lambda_p^2} \leq 1 \tag{5}$$

where λ_p is the element slenderness, defined as:

$$\lambda_p = \sqrt{\frac{f_y}{\sigma_{cr}}} = \frac{\bar{b}/t}{28.4\varepsilon\sqrt{k_\sigma}} \tag{6}$$

in which $\bar{b}/t$ is the relevant width-to-thickness ratio, k_σ is the buckling coefficient dependent on the boundary conditions and applied stress conditions, and ε is a material factor, defined as:

$$\varepsilon = \sqrt{\frac{235}{f_y}\frac{E_0}{210000}} \tag{7}$$

The overall buckling reduction factor χ can be calculated from Eqs. (8)-(10).

$$\chi = \frac{1}{\phi + \sqrt{\phi^2 - \lambda_c^2}} \leq 1 \tag{8}$$

$$\phi = 0.5[1 + \eta + \lambda_c^2] \tag{9}$$

$$\eta = \alpha(\lambda_c - \lambda_0) \tag{10}$$

in which the imperfection factor α and limiting slenderness λ_0 are taken as 0.49 and 0.40 respectively for welded compression members with hollow sections undergoing flexural buckling, and the non-dimensional slenderness λ_c, referred as the $\bar{\lambda}$ in EN 1993-1-4, can be defined by Eqs. (11) and (12).

$$\lambda_c = \sqrt{\frac{A f_y}{N_{cr}}} \qquad \text{for class 1, 2 and 3 cross-sections} \tag{11}$$

$$\lambda_c = \sqrt{\frac{A_{eff} f_y}{N_{cr}}} \qquad \text{for class 4 cross-sections} \tag{12}$$

where N_{cr} is the elastic global buckling load of the member.

Fig. 20 presents a comparison between the design strength curve predicted by EN 1993-1-4 and the test and FE results, in which the $N_{eff} = A_{eff} f_y$ represents the design resistance of the cross-section based on the effective area. It should be noted that two sets of the parameters n and e – (5.8, 0.0017) and (7.4, 0.0031) correspond to the data

points of stainless steel grades EN 1.4301 and EN 1.4462, respectively. For the grade EN 1.4301 columns, the mean value of $N_{b,Rd}/N_u$ is 1.06 with a corresponding COV of 0.05, while for the grade EN 1.4462 columns, the mean strength predictions and corresponding COV are 0.95 and 0.08, which means the columns of grade EN 1.4301 receive slightly overestimated strength predictions, while the columns of grade EN 1.4462 are generally slightly conservatively predicted.

6.3 Evaluation of the strength curves proposed by Rasmussen and Rondal

Rasmussen and Rondal [42] developed a general design approach for the buckling of columns made of nonlinear metallic materials, such as aluminium alloy and stainless steel, by introducing the non-dimensional proof stress $e = \sigma_{0.2}/E_0$ and the Ramberg-Osgood strain hardening exponent n into the strength formulations. The imperfection term, $\eta = \alpha(\lambda_c - \lambda_0)$, in Eq. (9) was redefined as

$$\eta = \alpha((\lambda_c - \lambda_1)^\beta - \lambda_0)$$ (13)

in which α, β, λ_0, λ_1 are parameters that depend on e and n. This proposal has been incorporated into the Australian Standard for stainless steel structures AS/NZS 4673 [43].

By inputting the two sets of values of parameters n and e corresponding to the stainless steel grades EN 1.4301 and EN 1.4462, the design curves proposed by Rasmussen and Rondal were compared with the obtained test and numerical results (see Fig. 21). The influence of the parameters n and e is clearly evident in Fig. 21, where two distinct buckling curves, which show good agreements with the corresponding data points, are plotted. The mean value of design strength over numerical strength for grade EN 1.4301 specimens is 0.98, which is the same as that of the grade EN 1.4462 specimens, while the COV values are equal to 0.05 and 0.10, respectively. Therefore, it may be concluded that the above curves proposed by Rasmussen and Rondal can provide better predictions of the buckling capacity of welded stainless steel sections than the current EN 1993-1-4 provisions, but at the expense of more complicated formulae.

6.4 Evaluation of the DSM

The DSM is adopted in the North American Specification for the Design of Cold-Formed Steel Structural Members (AISI 2007) [44]. The local-overall buckling capacity of columns is determined by first considering the overall flexural buckling capacity, and then reducing this to account for local buckling. The nominal axial resistance N_{ce} for flexural buckling can be determined from Eq. (14)

$$N_{ce} = \begin{cases} \left(0.658^{\lambda_c^2}\right) A f_y & \text{for } \lambda_c \leq 1.5 \\ \left(\dfrac{0.877}{\lambda_c^2}\right) A f_y & \text{for } \lambda_c > 1.5 \end{cases}$$ (14)

where the non-dimensional slenderness λ_c can be defined by Eqs. (11) for cross-sections of any class. Accounting for local buckling, the nominal axial resistance N_{cl} is acquired by reducing the N_{ce} in accordance with Eq. (15).

$$N_{cl} = \begin{cases} N_{ce} & \text{for } \lambda_l \leq 0.776 \\ \left[\dfrac{1}{\lambda_l^{0.8}} - \dfrac{0.15}{\lambda_l^{1.6}}\right] N_{ce} & \text{for } \lambda_l > 0.776 \end{cases}$$ (15)

in which the non-dimensional local slenderness λ_l is given by:

$$\lambda_l = \sqrt{N_{ce} / N_{crl}}$$ (16)

where N_{crl} is the elastic critical local buckling load, which may be determined using the semi-analytical finite strip software CUFSM [45].

Comparisons of the above DSM strength curve for cold-formed carbon steel sections with the generated test and

numerical data on welded stainless steel box sections are shown in Fig. 22, revealing an average of 23% overestimation of capacity. The unconservative predictions are unsurprising since welded stainless steel box sections will typically contain more severe imperfections and residual stresses than cold-formed carbon steel sections, and will experience material non-linearity at lower stress levels. It should be emphasised that the sections considered in the present study are clearly outside the scope of the above described DSM formulations, and revised strength curves are required for this use.

Proposed revisions to the DSM for application to cold-formed stainless steel sections have been made by Huang and Young [22] and Becque et al. [15], separately. Based on test and FE data on stainless steel square and rectangular hollow sections, Huang and Young proposed that Eqs. (14) and (15) could be replaced by Eqs. (17) and (18).

$$
N_{ce} = \begin{cases} \left(0.877^{\lambda_c^2}\right) A f_y & \text{for } \lambda_c \leq 1 \\ \left(\dfrac{0.877}{\lambda_c^2}\right) A f_y & \text{for } \lambda_c > 1 \end{cases} \tag{17}
$$

$$
N_{cl} = \begin{cases} N_{ce} & \text{for } \lambda_l \leq 0.7 \\ \left[\dfrac{0.96}{\lambda_l^{0.82}} - \dfrac{0.14}{\lambda_l^2}\right] N_{ce} & \text{for } \lambda_l > 0.7 \end{cases} \tag{18}
$$

Comparisons between the test/FE results and the Huang and Young proposals are shown in Fig. 23. Similarly to the comparisons of Fig. 22, unconservative predictions for welded stainless steel box sections are revealed, which is again attributed to the high levels of imperfections and residual stresses.

Becque et al. [15] also modified the original DSM formulae, on the basis of 245 data points on stainless steel sections including lipped channels, I-sections and box sections. Two separate column strength curves, taking account of local buckling, were presented in the format of the EN 1993-1-4 design provisions and the Rasmussen and Rondal proposal, which is included in AS/NZS 4673 [43]. In their proposals, the nominal axial resistance N_{ce} for flexural buckling is calculated from Eq. (19)

$$
N_{ce} = \chi A f_y \tag{19}
$$

where following the EN 1993-1-4 provisions, the reduction factor χ is obtained from Eqs. (8)-(11), the nominal axial resistance N_{cl} considering local buckling is given by Eq. (20), and is denoted DSM-Becque-EN 1993-1-4 in Fig. 24.

$$
N_{cl} = \begin{cases} N_{ce} & \text{for } \lambda_l \leq 0.55 \\ \left[\dfrac{0.95}{\lambda_l} - \dfrac{0.22}{\lambda_l^2}\right] N_{ce} & \text{for } \lambda_l > 0.55 \end{cases} \tag{20}
$$

Following the AS/NZS 4673 provisions, the reduction factor χ can be determined from Eqs. (8), (9), (11) and (13), and the corresponding axial resistance N_{cl} allowing for local buckling is given by Eq. (21) and denoted as DSM-Becque-AS/NZS 4673 in Fig. 24.

$$
N_{cl} = \begin{cases} N_{ce} & \text{for } \lambda_l \leq 0.474 \\ \left[\dfrac{0.95}{\lambda_l^{0.8}} - \dfrac{0.22}{\lambda_l^{1.6}}\right] N_{ce} & \text{for } \lambda_l > 0.474 \end{cases} \tag{21}
$$

Comparisons between the Becque et al. strength curves and the obtained test and FE results are shown in Fig. 24. The average ratios of predicted to test/FE strengths are 1.04 and 1.03 for the recommendations in the EN 1993-1-4 and the AS/NZS 4673 formats, respectively. A lower scatter of the predictions is achieved in the latter case due to the consideration of the material parameters n and e. Both of the Becque et al. proposals provide good predictions of the test/FE results, but are marginally unconservative on average. Hence possible modifications are proposed in the

following sub-sections.

6.5 Design proposals

The above comparisons have highlighted shortcomings in existing column design provisions in both the EN 1993-1-4 and DSM formats. Primarily, this relates to the fact that the design formulae were developed on the basis of relatively few test data or different section types to those considered herein. Modified design formulae in the EN 1993-1-4 and DSM formats for welded stainless steel sections are therefore proposed in this sub-section.

6.5.1 Modification to the EN 1993-1-4 provisions

Based on the obtained test and numerical results, two sets of values for the imperfection factor α and limiting slenderness λ_0 are proposed separately for the austenitic and duplex grades in Table 7, which have been verified against the following ranges of the exponent n and the parameter e: austenitic grades – n= 5.8-9.0, e=0.0011-0.0018; duplex grades – n= 5.0-7.5, e=0.0021-0.0035. Compared to the austenitic grades, a lower imperfection factor α but a higher value of λ_0 was assigned to the duplex grades, which can be attributed to their lower sensitivity to geometric imperfections and lower residual stress ratios.

6.5.2 Modification to the DSM

In the DSM format, the following revised formulae for determining the nominal axial resistance of welded stainless steel sections N_{cl}, accounting for local buckling, are proposed:

$$N_{cl} = \begin{cases} N_{ce} & \text{for } \lambda_l \leq 0.474 \\ \left[\dfrac{0.86}{\lambda_l^{0.8}} - \dfrac{0.17}{\lambda_l^{1.6}} \right] N_{ce} & \text{for } \lambda_l > 0.474 \end{cases} \tag{22}$$

6.5.3 Assessment of design proposals

The new design proposals are assessed by means of comparison with the obtained test and numerical results, as illustrated in Figs. 25 and 26. The mean values of strength prediction ratios (Predicted/Test(FE)) and the corresponding values of COV are listed for both the existing design methods and the new design proposals in Table 8. The accuracy of the strength predictions, may be seen to improve by applying the new design proposals. Specifically, the modified EN 1993-1-4 offers mean strength prediction ratios of 0.99 and 1.00 for austenitic and duplex stainless steels, respectively, with the same COV of 0.06. The modified DSM predicts 99% of the test and numerical strengths on average, with a COV of 0.06. It can be concluded that the obtained test and numerical results on welded stainless steel sections may be accurately predicted by the proposed buckling curves.

7. Conclusions

The local-overall interactive buckling resistances of welded stainless steel columns with box sections have been investigated experimentally and numerically in this study. Eight interactive buckling tests on welded stainless steel SHS and RHS columns of the grades EN 1.4301 and EN 1.4462 were performed. Based on the obtained experimental results, FE models were generated and carefully validated.

Using the validated FE models, parametric studies were conducted to investigate the interaction between local and overall flexural buckling, covering a wide range of both local and global slenderness, with other key parameters, such as the residual stresses, strain hardening exponent, non-dimensional proof stress, and geometric imperfections, taken into consideration. The obtained test and numerical results were used to assess existing design methods, including the design provisions of EN 1993-1-4, the proposals of Rasmussen and Rondal, the DSM for cold-formed carbon steel and two revised versions thereof. The current EN 1993-1-4 buckling formulae do not differ with grade, leading to satisfactory average strength predictions but slightly overestimated and slightly underestimated predicted capacities for austenitic and duplex stainless steel sections, respectively. The three DSM curves, which were developed for cold-formed sections rather than the welded stainless steel sections, were also evaluated; the Becque et

al. proposals were found to provide acceptable strength predictions for the sections considered herein, but modified proposals to achieve improved accuracy were also sought.

Based on the obtained test and numerical results, modifications to the current EN 1993-1-4 design formulae and the DSM have been proposed. Two separate sets of imperfection factor and limiting slenderness were presented for the modified EN 1993-1-4 buckling curves, to cover the austenitic and duplex stainless steels. The key parameters in the DSM were also adjusted. The revised proposals are shown to provide accurate predictions for the interactive buckling resistances of welded stainless steel box section compression members.

Acknowledgements

References

[1] Gardner L. The use of stainless steel in structures. Prog Struct Eng Mater 2005;7(2):45-55.
[2] Svensson SE, Croll JGA. Interaction between local and overall buckling. International Journal of Mechanical Sciences 1975;17(4):307-321.
[3] van der Neut A. The interaction of local buckling and column failure of thin-walled compression members. Proceedings of the 12th International Congress on Applied Mechanics; 1969. p. 389-399.
[4] Wadee MA, Gardner L. Cellular buckling from mode interaction in I-beams under uniform bending. Proceedings of the Royal Society A: Mathematical, Physical and Engineering Science 2012;468(2137):245-268.
[5] Rasmussen KJR, Hancock GJ. Design of cold-formed stainless steel tubular members. I: Columns. J Struct Eng, ASCE 1993;119(8):2349-2367.
[6] Young B, Hartono W. Compression tests of stainless steel tubular members. J Struct Eng, ASCE 2002;128(6):754-761.
[7] Theofanous M, Chan TM, Gardner L. Structural response of stainless steel oval hollow section compression members. Eng Struct 2009;31(4):922-934.
[8] Theofanous M, Gardner L. Testing and numerical modelling of lean duplex stainless steel hollow section columns. Eng Struct 2009;31(12):3047-3058.
[9] Kuwamura H. Local buckling of thin-walled stainless steel members. Steel Struct 2003;3: 191-201.
[10] Liu Y, Young B. Buckling of stainless steel square hollow section compression members. J Constr Steel Res 2003;59(2):165-177.
[11] Gardner L, Nethercot DA. Experiments on stainless steel hollow sections – part 1: Material and cross-sectional behaviour. J Constr Steel Res 2004;60(9):1291-1318.
[12] Young B, Lui W M. Tests of cold-formed high strength stainless steel compression members. Thin Wall Struct 2006;44(2):224-234.
[13] Becque J, Rasmussen KJR. Experimental investigation of local-overall interaction buckling of stainless steel lipped channel columns. J Constr Steel Res 2009;65(8):1677-1684.
[14] Becque J, Rasmussen KJR. Experimental investigation of the interaction of local and overall buckling of stainless steel I-columns. J Struct Eng, ASCE 2009;135(11):1340-1348.
[15] Becque J, Lecce M, Rasmussen KJR. The direct strength method for stainless steel compression members. J Constr Steel Res 2008;64(11):1231-1238.
[16] Rossi B, Jaspart JP, Rasmussen KJR. Combined distortional and overall flexural-torsional buckling of cold-formed stainless steel sections: Experimental investigations. J Struct Eng, ASCE 2010; 136(4):354-360.
[17] Rossi B, Jaspart JP, Rasmussen K J R. Combined distortional and overall flexural-torsional buckling of cold-formed stainless steel sections: Design. J Struct Eng, ASCE 2010;136(4):361-369.
[18] Gonçalves R, Camotim D. GBT local and global buckling analysis of aluminium and stainless steel columns. Computers and Structures 2004;82(17):1473-1484.
[19] EN 1993-1-4. Eurocode 3: Design of steel structures – Part 1.4: General rules–Supplementary rules for stainless steels. CEN. 2006.
[20] Schafer BW, Peköz T. Direct strength prediction of cold-formed steel members using numerical elastic buckling solutions. *Proceedings of the fourteenth international specialty conference on cold-formed steel structures*. St. Louis, Missouri, October 15-16, 1998.
[21] Schafer BW. Review: the direct strength method of cold-formed steel member design. J Constr Steel Res 2008;64(7):766-778.
[22] Huang Y, Young B. Direct strength method and continuous strength method for cold-formed lean duplex stainless steel columns. *Research and Applications in Structural Engineering, Mechanics and Computation*, London, UK. Taylor & Francis Group, 2013: 1441-1446.
[23] Yuan HX, Wang YQ, Shi YJ, Gardner L. Stub column tests on stainless steel built-up sections. Thin Wall Struct 2014:83:103-114.
[24] Ban HY, Shi G, Shi YJ, Wang YQ. Overall buckling behavior of 460 MPa high strength steel columns: experimental investigation

and design method. J Constr Steel Res 2012;74:140-150.

[25] European Convention for Constructional Steelworks, ECCS. Manual on stability of steel structures – Part 2.2 Mechanical properties and residual stresses. 2nd Edition, Bruxelles: ECCS Publ., 1976.

[26] Yuan HX, Wang YQ, Shi YJ, Gardner L. Residual stress distributions in welded stainless steel sections, Thin Wall Struct 2014;79:38-51.

[27] Ziemian RD. Guide to stability design criteria for metal structures. 6th ed. New York: John Wiley & Sons, Inc., 2010.

[28] Vann WP, Sehested J. Experimental techniques for plate buckling. *Proceedings of the 2nd Specialty Conference on Cold – Formed Steel Structures*. USA: University of Missouri – Rolla, October 22-24, 1973.

[29] Rossmen CA, Bsrtone LM, Dobrowski CV. Compressive strength of flat panels with Z-section stiffeners. National Advisory Committee for Aeronautics (NACA), Advance Restricted Report No. 4B03, 1944.

[30] Hu PC, Lundquist EE, Batdorf SB. Effect of small deviations from flatness on effective width and buckling of plates in compression. National Advisory Committee for Aeronautics (NACA), Technical Note No. 1124, 1946.

[31] van den Berg GJ. The effect of the non-linear stress–strain behaviour of stainless steels on member capacity. J Constr Steel Res 2000;54(1):135-160.

[32] Hibbitt H, Karlsson B, Sorensen P. ABAQUS Analysis User's Manual Version 6.10. Dassault Systèmes Simulia Corp.: Providence, RI, USA, 2011.

[33] Gardner L, Ashraf M. Structural design for non-linear metallic materials. Eng Struct 2006;28(6):926-934.

[34] Saliba N, Gardner L. Experimental study of the shear response of lean duplex stainless steel plate girders. Eng Struct 2013;46:375-391.

[35] Zhou F, Young B. Web crippling behaviour of cold-formed duplex stainless steel tubular sections at elevated temperatures. Eng Struct 2013;57:51-62.

[36] Hassanein M F. Imperfection analysis of austenitic stainless steel plate girders failing by shear. Eng Struct 2010;32(3):704-713.

[37] Gardner L, Nethercot DA. Numerical modeling of stainless steel structural components – a consistent approach. J Struct Eng, ASCE 2004;130(10):1586-1601.

[38] Ellobody E, Young B. Structural performance of cold-formed high strength stainless steel columns. J Constr Steel Res 2005;61(12):1631-1649.

[39] Jandera M, Gardner L, Machacek J. Residual stresses in cold-rolled stainless steel hollow sections. J Constr Steel Res 2008;64(11):1255-1263.

[40] EN 1993-1-5. Eurocode 3: Design of steel structures – Part 1.5: Plated structural elements. CEN. 2006.

[41] Rusch A, Lindner J. Remarks to the direct strength method. Thin Wall Struct 2001;39(9):807-820.

[42] Rasmussen KJR, Rondal J. Strength curves for metal columns. J Struct Eng, ASCE 1997;123(6):721-728.

[43] AS/NZS 4673. Cold-formed stainless steel structures. Sydney: Standards Australia, 2001.

[44] AISI. North American Specification for the design of cold-formed steel structural members. AISI S100-2007, North American Cold-formed Steel Specification, American Iron and Steel Institute (AISI), Washington D.C., 2007.

[45] Li Z, Schafer BW. Buckling analysis of cold-formed steel members with general boundary conditions using CUFSM: conventional and constrained finite strip methods. *Proceedings of the 20th Intl. Spec. Conf. on Cold-Formed Steel Structures*, St. Louis, MO. November, 2010.
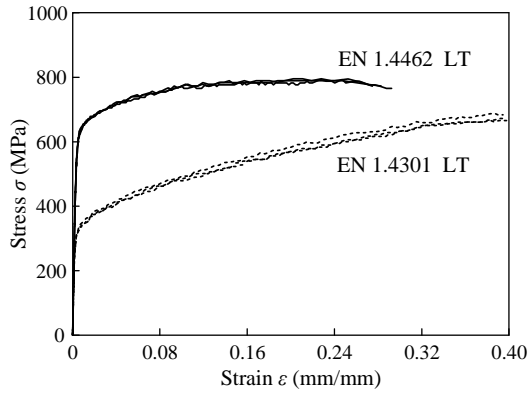
(a) Tension
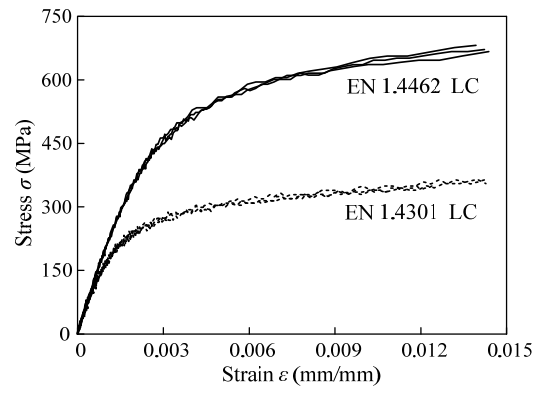
(b) Compression

Fig. 1. Measured full stress-strain curves (3 repeated tests per specimen)
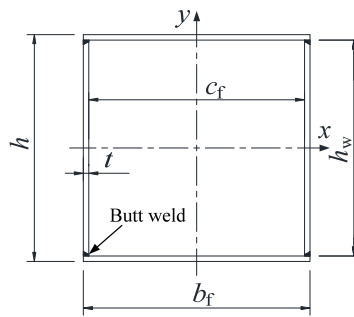
Fig. 2. Geometry and notation for test specimens
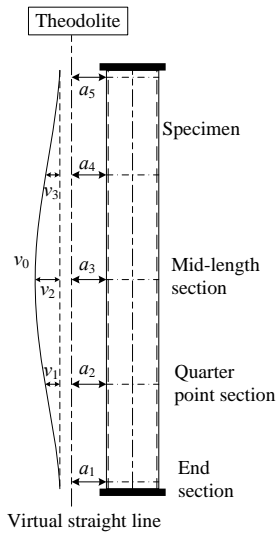
(a) Schematic view
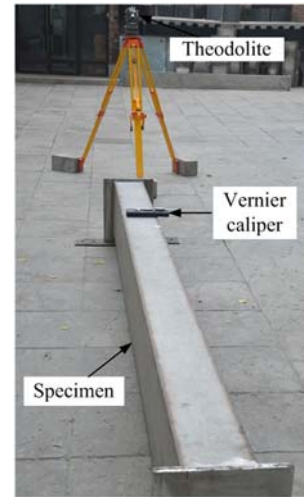
(b) Field measurement

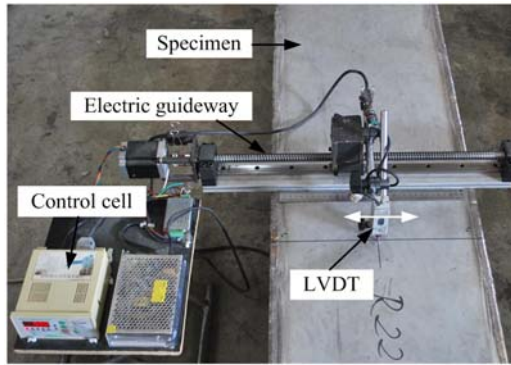**Fig. 3.** Measurement of initial global geometric imperfection amplitudes

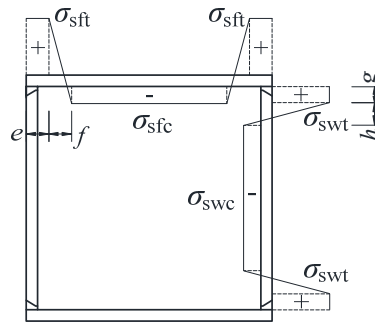**Fig. 4.** Determination of initial local geometric imperfections

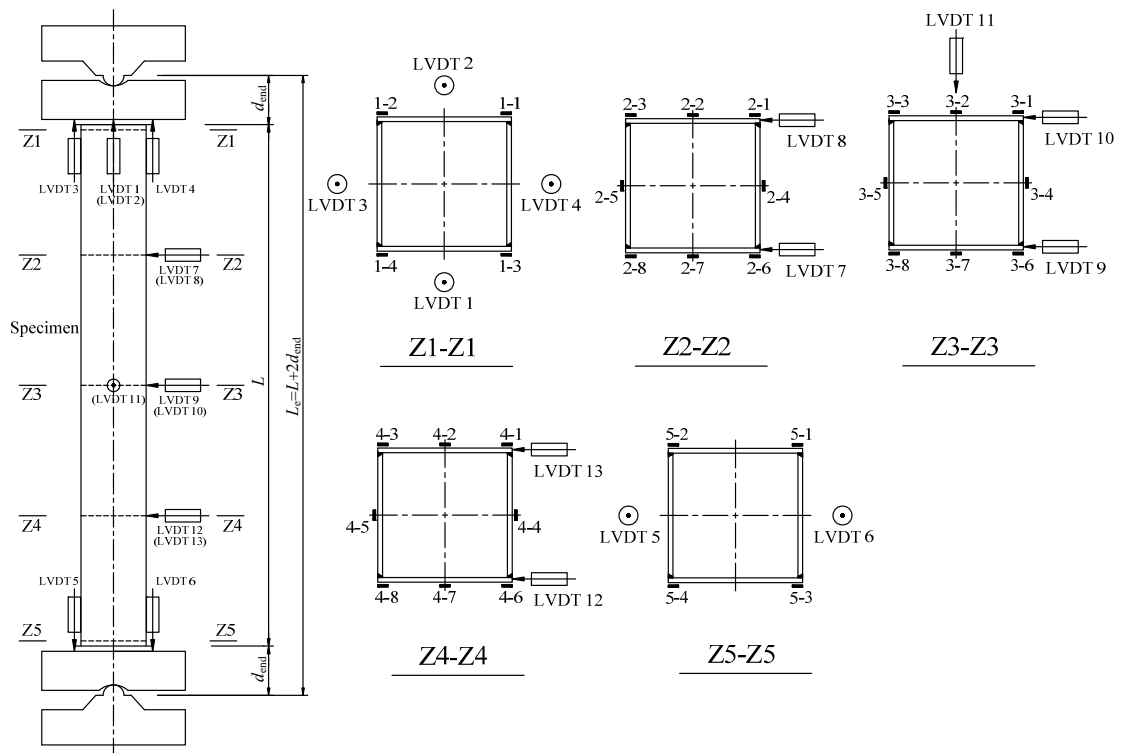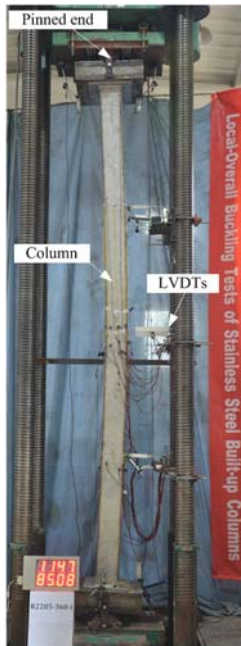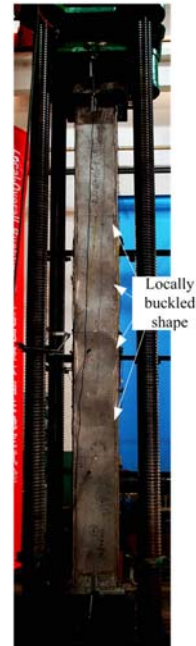**Fig. 5.** Residual stress pattern in welded stainless steel box sections

Fig. 6. Instrumentation configurations for test specimens

(a) Front view   (b) Lateral view

Fig. 7. Test set-up for local-overall buckling tests (R2205-360-i)
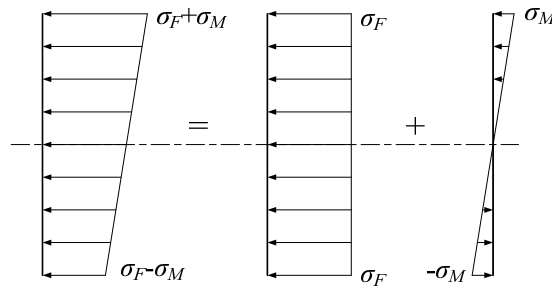
Fig. 8. Stress state of a column section subjected to eccentric loading

Fig. 9. Deformed shapes of all test specimens
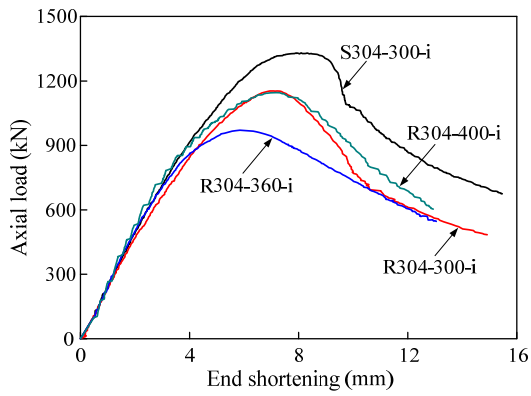
(a) Axial load versus end shortening
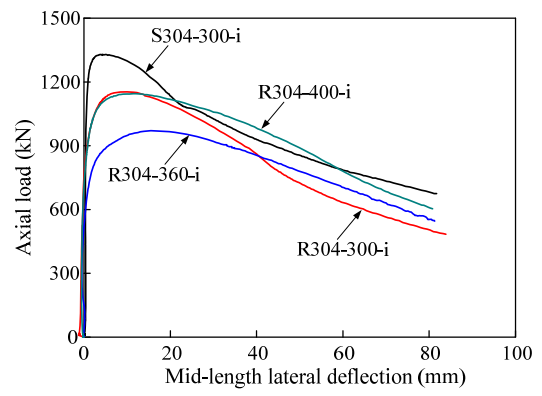
(b) Axial load versus mid-length lateral deflection

Fig. 10. Axial load versus deformation curves for grade EN 1.4301 test specimens
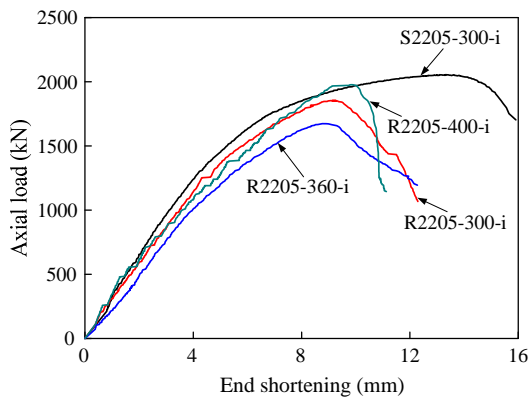
(a) Axial load versus end shortening
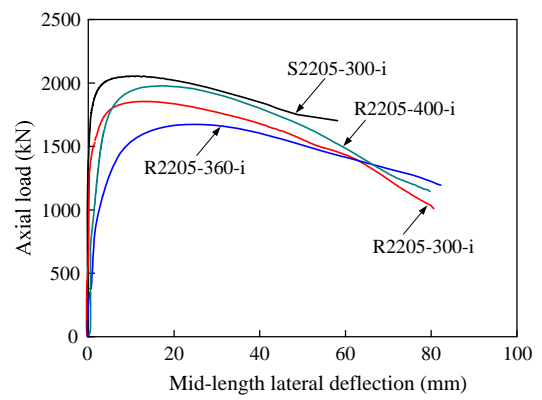
(b) Axial load versus mid-length lateral deflection

Fig. 11. Axial load versus deformation curves for grade EN 1.4462 test specimens
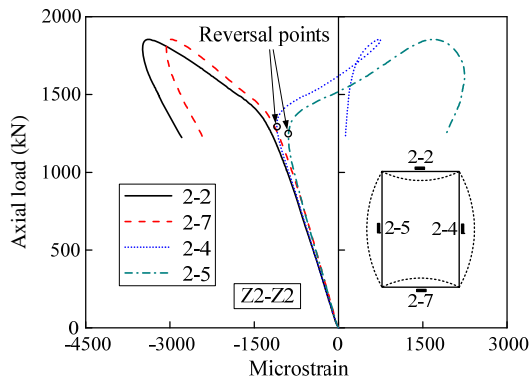
(a) Upper quarter point cross section
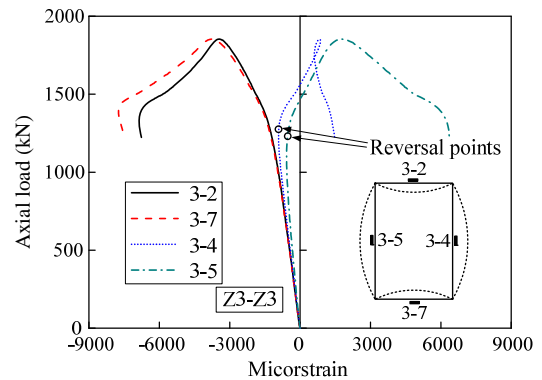
(b) Mid-length cross section
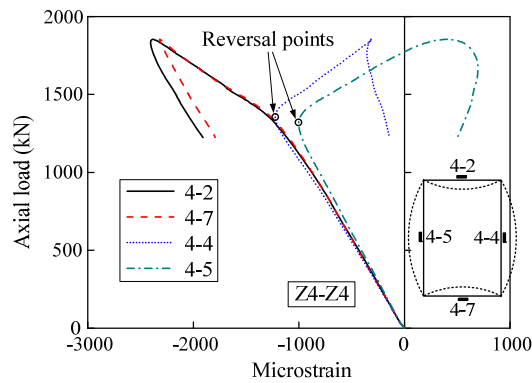
(c) Lower quarter point cross section

Fig. 12. Axial load versus surface microstrain curves for the specimen R2205-300-i
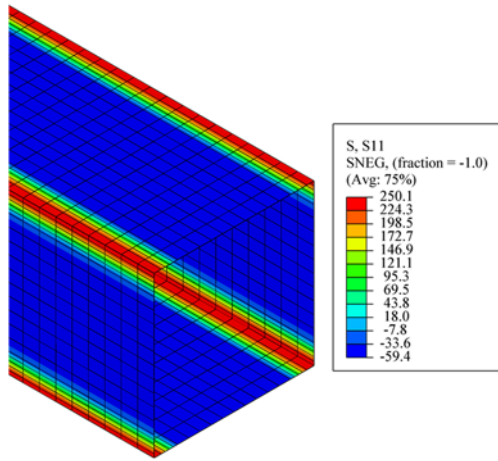
(a) S304-300-i
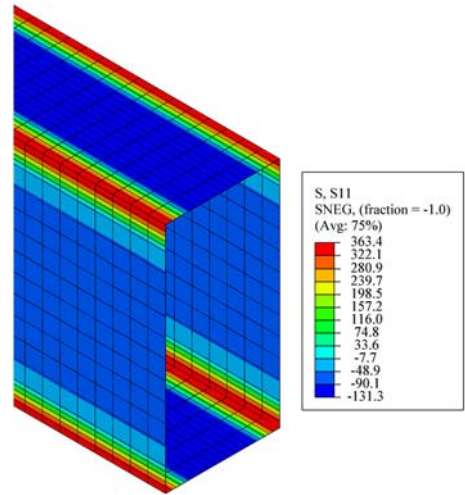
(b) R2205-400-i

Fig. 13. Distribution of residual stresses in FE models
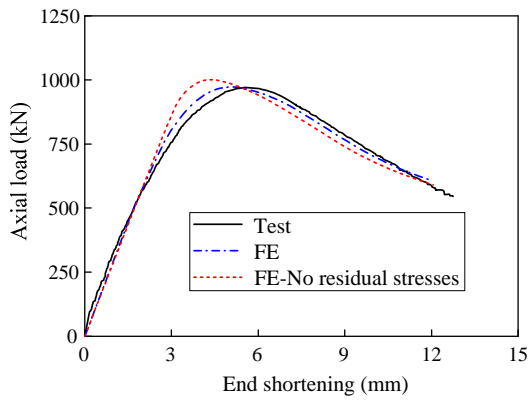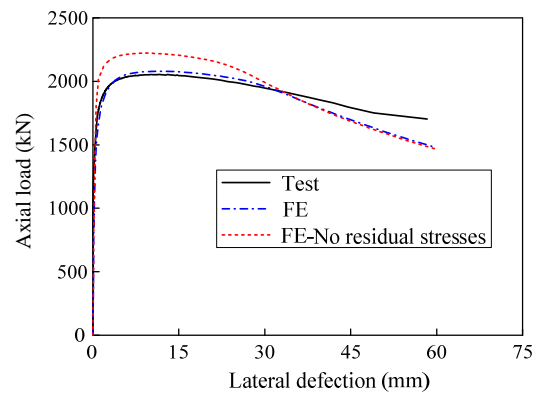

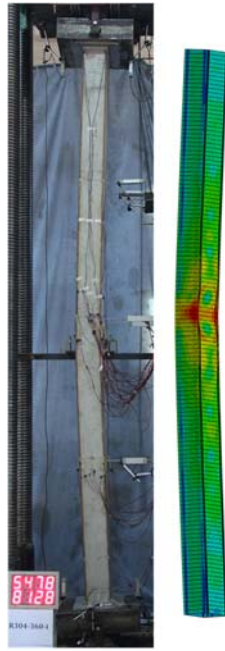
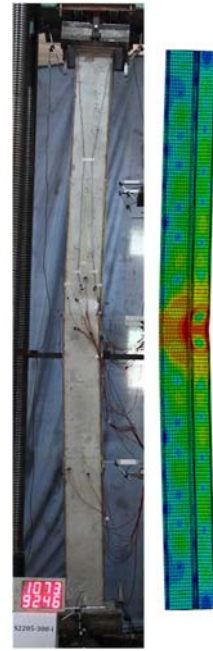(a) R304-360-i
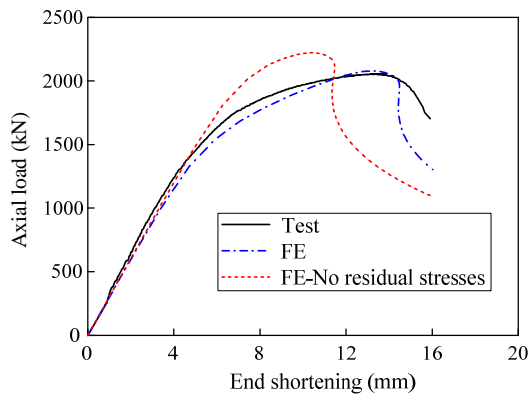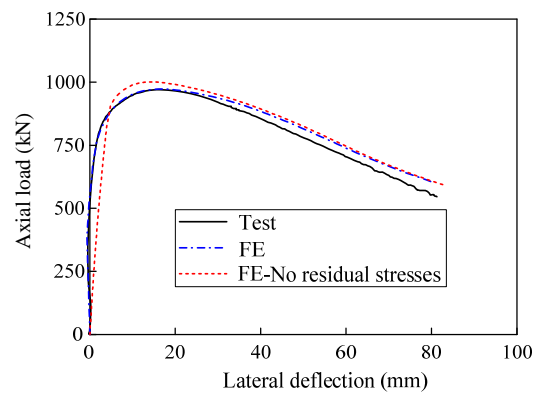
(b) S2205-300-i

Fig. 14. Comparison between test and FE load-deformation curves
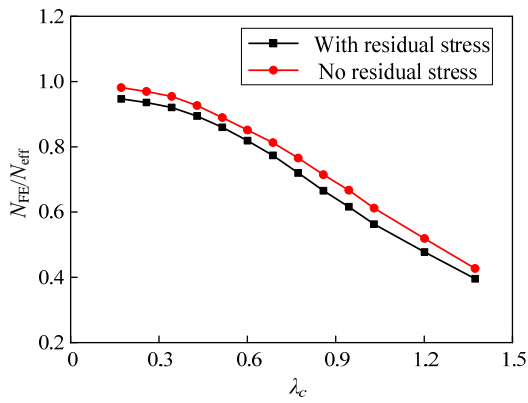
5
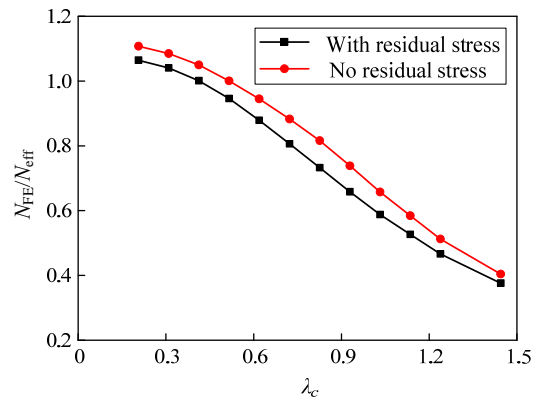
(a) R304-360-i   (b) S2205-300-i

Fig. 15. Comparison of failure modes from the interactive buckling tests and FE modelling
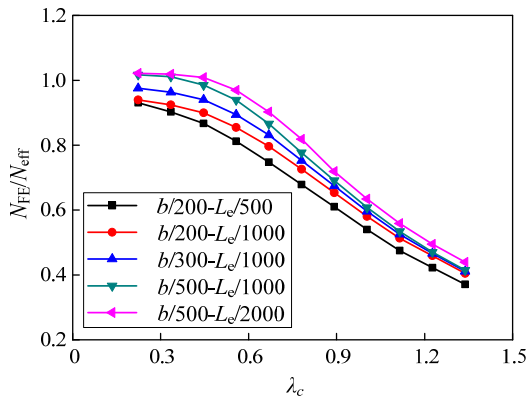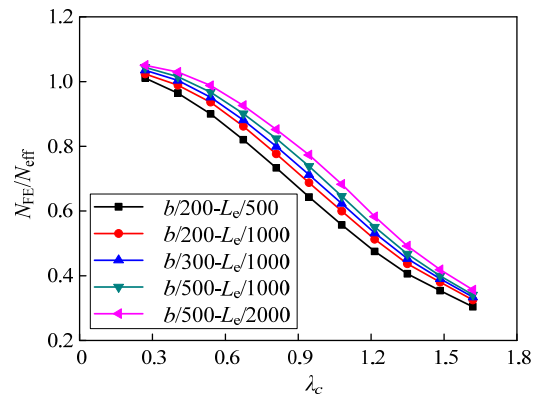

(a) Grade EN 1.4301   (b) Grade EN 1.4462

Fig. 16. Influence of the residual stresses on interactive buckling capacity
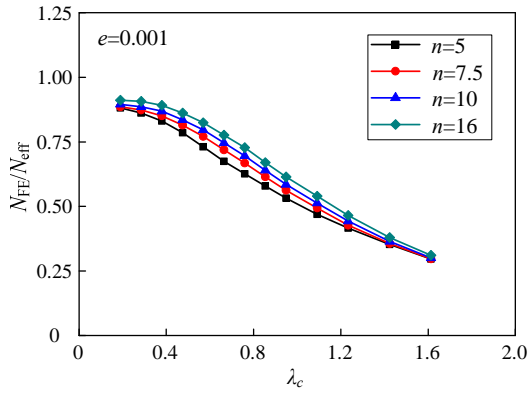

(a) Grade EN 1.4301   (b) Grade EN 1.4462

Fig. 17. Influence of initial local and global geometric imperfections on interactive buckling capacity
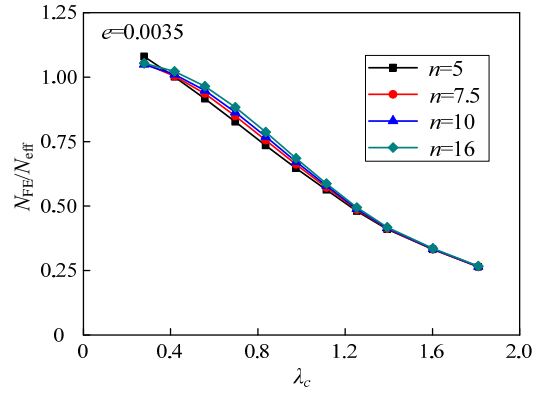
(a) e=0.001   (b) e=0.0035

Fig. 18. Influence of the strain hardening exponent n

(a) n=5   (b) n=16

Fig. 19. Influence of the non-dimensional proof stress e

Fig. 20. Comparison of test and FE results with the EN 1993-1-4 design curve
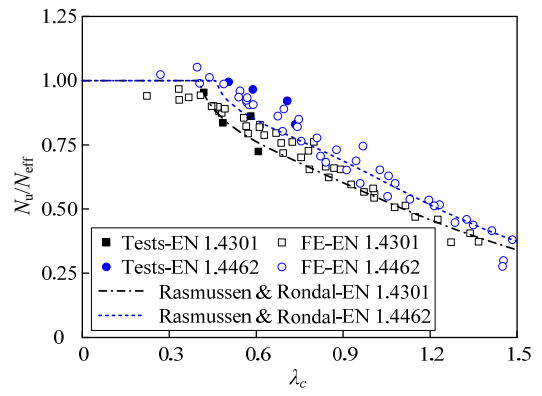
Fig. 21. Comparison of test and FE results with the Rasmussen and Rondal proposed curves
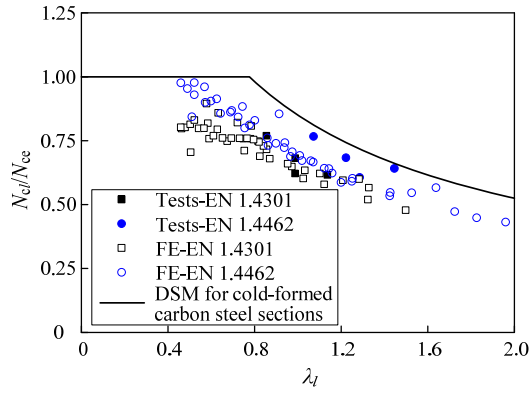
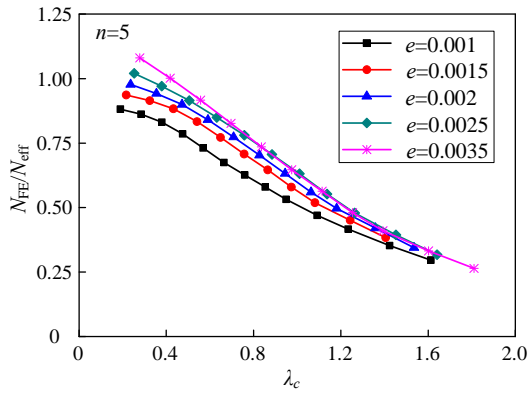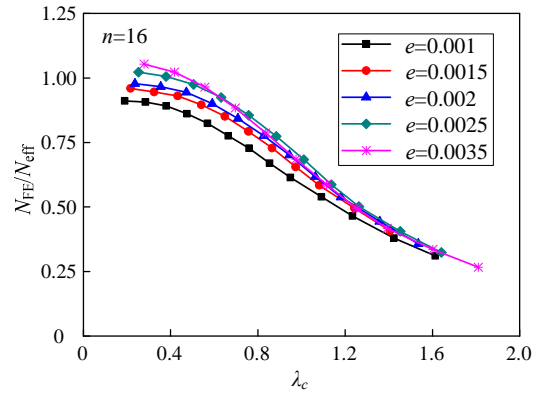**Fig. 22.** Comparison of test and FE results with the DSM design curve for cold-formed carbon steel sections [44]
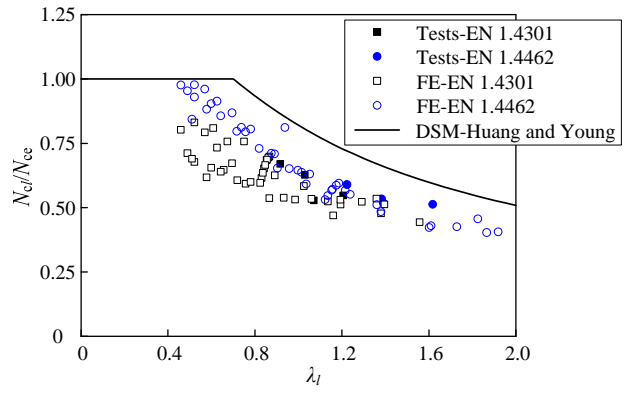
Fig. 23. Comparison of test and FE results with the DSM design curve from Huang and Young [22] for cold-formed stainless steel sections
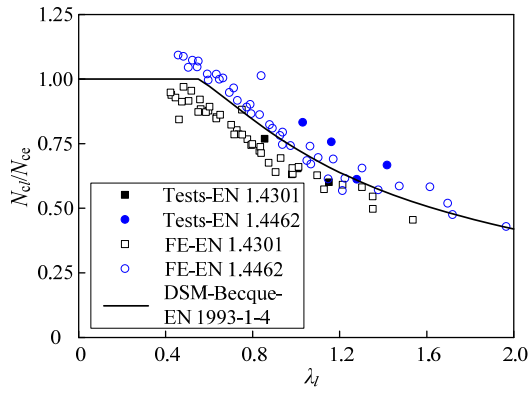
(a) DSM-Becque-EN 1993-1-4 format
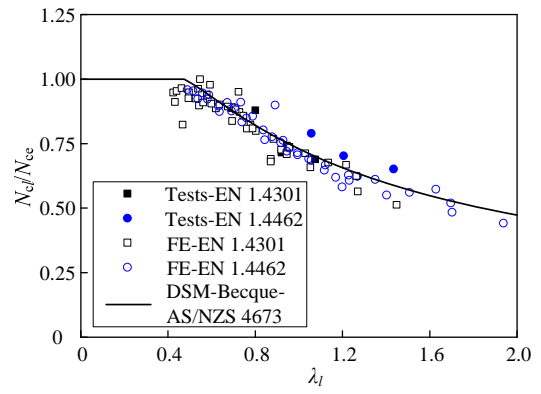
(b) DSM-Becque-AS/NZS 4673 format

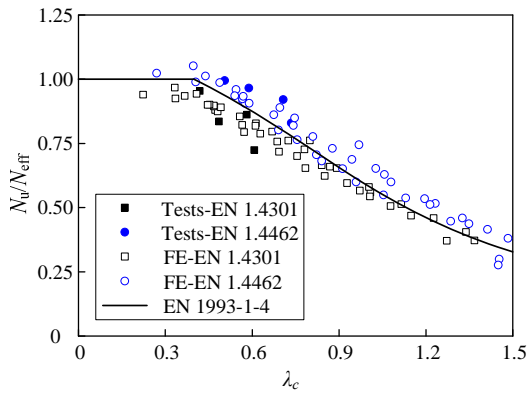**Fig. 24.** Comparison of test and FE results with the DSM design curves from Becque et al. [15]
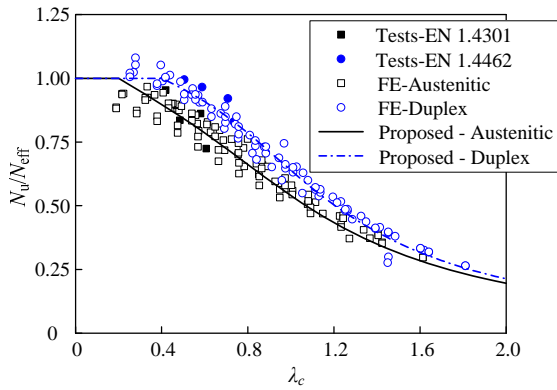
Fig. 25. Comparison of test and FE results with the modified EN 1993-1-4 design curves
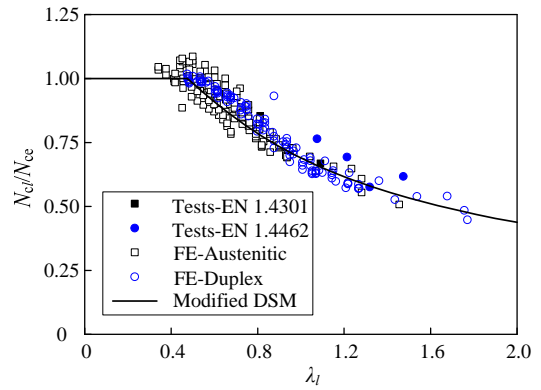
Fig. 26. Comparison of test and FE results with the modified DSM design curve

Table 1

Measured material properties from hot-rolled coil used to fabricate structural sections

Grade	t (mm)	Direction	E_0 (MPa)	$\sigma_{0.01}$ (MPa)	$\sigma_{0.2}$ (MPa)	$\sigma_{1.0}$ (MPa)	σ_u (MPa)	ε_f (%)	n
1.4301	6.00	LT	188600	186.3	312.6	354.4	695.7	60.6	5.8
		LC	182300	177.2	281.5	347.3	-	-	6.5
1.4462	6.00	LT	193200	404.4	605.6	665.0	797.9	34.6	7.4
		LC	191900	360.6	553.0	667.4	-	-	7.0

LT: Longitudinal Tension, LC: Longitudinal Compression.

Table 2

Measured geometric dimensions of the test specimens

| Specimen	b_f (mm)	h (mm)	$t_f=t_w=t$ (mm)	A (mm^2)	h/b_f	c_f/t	h_w/t	L (mm)	L_e (mm)	L_e/r_y	λ_{pf}	λ_{pw}	λ_c
S304-300-i	299.8	300.0	6.0	7053.4	1.0	48.0	48.0	4497.3	4877.3	40.7	1.03	1.03	0.42
R304-300-i	200.5	300.1	6.0	5863.1	1.5	31.4	48.0	3998.0	4378.0	52.5	0.67	1.03	0.58
R304-360-i	179.8	360.2	6.0	6336.6	2.0	28.0	58.0	3998.6	4378.6	57.0	0.60	1.24	0.61
R304-400-i	200.4	400.3	6.0	7064.4	2.0	31.4	64.7	3702.7	4082.7	47.5	0.67	1.39	0.49
S2205-300-i	299.0	300.6	6.0	7050.4	1.0	47.8	48.1	4497.7	4877.7	40.7	1.41	1.42	0.51
R2205-300-i	199.7	300.0	6.0	5852.8	1.5	31.3	48.0	3996.2	4376.2	52.7	0.92	1.41	0.71
R2205-360-i	180.1	360.5	6.0	6342.8	2.0	28.0	58.1	3997.8	4377.8	56.9	0.83	1.71	0.74
R2205-400-i	199.5	400.2	6.0	7052.4	2.0	31.3	64.7	3697.5	4077.5	47.7	0.92	1.91	0.59

Table 3

Measured initial geometric imperfection amplitudes and load eccentricities of the test specimens

Specimen	w_0 (mm)	v_0 (mm)	e_c (mm)	e_{Eq} (mm)	e_{Eq}/L
S304-300-i	0.62	1.58	1.75	3.33	1/1350
R304-300-i	0.58	-1.96	5.49	3.52	1/1134
R304-360-i	0.69	-0.94	11.10	10.16	1/394
R304-400-i	0.62	0.28	-4.16	-3.87	1/956
S2205-300-i	0.53	0.56	0.56	1.12	1/4021
R2205-300-i	0.65	0.72	-1.27	-0.55	1/7223
R2205-360-i	0.78	-0.11	-2.36	-2.47	1/1618
R2205-400-i	1.12	-1.42	2.29	0.86	1/4282

Table 4

Key parameters in the proposed models for residual stresses in welded stainless steel box sections

Alloy	Ratio	$\sigma_{sft}=\sigma_{swt}$	e	f	g	h
Austenitic	$h/t(b_f/t)<20$	$0.8\sigma_{0.2}$	0	$5t_f$	0	$5t_w$
	$h/t(b_f/t)\geq20$	$0.8\sigma_{0.2}$	$t_w+0.025c_f$	$5t_f$	$0.025h_w$	$5t_w$
Duplex	$h/t(b_f/t)<20$	$0.6\sigma_{0.2}$	0	$5t_f$	0	$5t_w$
	$h/t(b_f/t)\geq20$	$0.6\sigma_{0.2}$	$t_w+0.025c_f$	$5t_f$	$0.025h_w$	$5t_w$

Table 5

Comparison between experimental and FE results

Specimen	$N_{u,Exp}$ (kN)	$\delta_{u,Exp}$ (mm)	$\Delta_{u,Exp}$ (mm)	FE results with residual stresses						FE results without residual stresses		
				$N_{u,FE}$ (kN)	$\delta_{u,FE}$ (mm)	$\Delta_{u,FE}$ (mm)	$N_{u,FE}/N_{u,Exp}$	$\delta_{u,FE}/\delta_{u,Exp}$	$\Delta_{u,FE}/\Delta_{u,Exp}$	$N_u/N_{u,Exp}$	$\delta_u/\delta_{u,Exp}$	$\Delta_u/\Delta_{u,Exp}$
S304-300-i	1330.1	8.1	4.4	1338.8	7.5	6.7	1.01	0.93	1.54	1.06	0.80	1.51
R304-300-i	1153.3	6.9	9.6	1178.3	6.1	12.2	1.02	0.88	1.27	1.02	0.79	1.36
R304-360-i	970.3	5.5	15.5	972.5	5.1	16.2	1.00	0.93	1.04	1.03	0.78	0.90
R304-400-i	1145.2	7.0	12.0	1188.0	5.5	13.9	1.04	0.79	1.16	1.06	0.64	0.88
S2205-300-i	2054.1	13.1	9.7	2078.5	13.2	11.3	1.01	1.01	1.17	1.08	0.79	0.95
R2205-300-i	1853.6	9.3	13.4	1802.7	8.4	14.6	0.97	0.91	1.09	1.06	0.82	0.56
R2205-360-i	1673.3	8.8	23.7	1597.5	7.4	24.7	0.95	0.84	1.04	1.04	0.75	0.57
R2205-400-i	1976.6	9.8	15.7	1963.1	8.8	15.7	0.99	0.90	1.00	1.03	0.76	0.76
Mean	-	-	-	-	-	-	**1.00**	**0.90**	**1.16**	**1.05**	**0.77**	**0.94**
COV	-	-	-	-	-	-	**0.02**	**0.06**	**0.16**	**0.02**	**0.05**	**0.32**

Table 6

Critical local buckling loads of the test specimens

Specimen	$N_{crl,Exp}$ (kN)	$\sigma_{crl,Exp}$ (MPa)	FE results $\sigma_{crl,FE}$ (MPa)	$\sigma_{crl,FE}/\sigma_{crl,Exp}$
S304-300-i	**1153.8**	**163.6**	135.0	0.83
R304-300-i	**1010.6**	**172.4**	166.6	0.97
R304-360-i	**630.6**	**99.5**	105.9	1.06
R304-400-i	**516.8**	**73.2**	92.0	1.26
S2205-300-i	**1210.6**	**171.7**	140.7	0.82
R2205-300-i	**1084.8**	**185.3**	176.2	0.95
R2205-360-i	**799.0**	**126.0**	152.5	1.21
R2205-400-i	**541.8**	**76.8**	68.1	0.89

Table 7

Values of the parameters related to the modified EN 1993-1-4 column buckling curves

Parameters	α	λ_0
Austenitic grades	0.49	0.20
Duplex grades	0.34	0.40

Table 8

Comparison of strength prediction ratios for the considered design methods and proposals (Predicted/Test(FE))

Index	Existing design methods/proposals								New design proposals		
	EN 1993-1-4 [19]		Rasmussen and Rondal [42]		DSM				Modified EN 1993-1-4		
						Becque et al. [15]		Huang and Young [22]			Modified DSM
	Austenitic	Duplex	Austenitic	Duplex	DSM for carbon steel [44]	EN 1993-1-4	AS/NZS 4673		Austenitic	Duplex	
Mean	1.06	0.95	0.98	0.98	1.23	1.04	1.03	1.33	**0.99**	**1.00**	**0.99**
COV	0.05	0.08	0.05	0.10	0.09	0.10	0.08	0.15	**0.06**	**0.06**	**0.06**